Available online at www.sciencedirect.com
ScienceDirect
Catalysis Today 125 (2007) 2–10
CATALYSIS TODAY
www.elsevier.com/locate/cattod

Preparation of Pt/ZSM-5 films on stainless steel microreactors

O. de la Iglesia [a], V. Sebastián [a], R. Mallada [a], G. Nikolaidis [b], J. Coronas [a], G. Kolb [b], R. Zapf [b], V. Hessel [b], J. Santamaría [a,*]

[a] *Department of Chemical and Environmental Engineering, University of Zaragoza, Zaragoza, Spain*
[b] *Institut für Mikrotechnik Mainz GmbH, Mainz, Germany*

Available online 2 May 2007

Abstract

Different synthesis methods (seeded and unseeded liquid phase hydrothermal synthesis, steam-assisted crystallization) have been employed to prepare zeolite films as catalytic coatings on the channels of stainless steel microreactors. The best results were obtained using seeded steam-assisted crystallization (SAC) which under suitable conditions led to well-crystallized zeolite films whose growth was confined to the channel spaces. Liquid phase synthesis yielded higher catalyst loads but was less effective in confining crystal growth to the desired regions. Once the zeolite films were formed, conventional ion-exchange procedures were used to produce a homogeneous distribution of Pt in the zeolite films.

Keywords: Microreactors; Zeolite films; Zeolite synthesis methods

1. Introduction

In recent years, microstructured reactors have become one of the most active research areas in catalysis and reaction engineering, as witnessed by several review papers on this subject [1–7]. Microstructured reactors are three-dimensional structures with inner dimensions measured in tens to hundreds of microns [5]. The main feature of microreactors is their high surface area to volume ratio, with values between 5000 and 50,000 $m^2\ m^{-3}$, while those of traditional reactors are about 100 $m^2\ m^{-3}$, reaching values of 1000 $m^2\ m^{-3}$ only in exceptional cases. The enhancement of transport properties in microreactors produces high heat transfer rates, allowing for instance to carry out highly exothermic reactions under near-isothermal conditions [8]. The avoidance of hot spots not only results in a safer operation, but also helps to suppress undesirable side reactions, leading to higher selectivity, yield, and product quality. In addition, mass transfer processes can also be accelerated considerably in microreactors because of their small dimensions. This means that it is possible to strongly reduce diffusion times in microreactors, thus reducing the mass-transfer limited operating region. Finally, process parameters such as pressure, temperature and residence time are more easily controlled in reactions that take place in small volumes. The potential hazard of strongly exothermic or explosive reactions could be drastically reduced and the same can be said of processes that operate with toxic substances or under high operating pressures, where a microreactor offers higher safety levels than conventional reactors [9].

The above mentioned properties also make microreactors suitable as process engineering tools for acquiring kinetic and design data useful for scaling up new processes and for the optimization of those already in operation [10]. Microreactors also give opportunities for new production concepts: depending on demand, several microreactors could be stacked in parallel to achieve the desired product output, thus achieving a flexible production capacity.

Catalytic activity has been introduced into microreactors by loading noble metals (e.g. Pt [11], Pd [12]) or mixtures of metals or metal oxides (e.g. [13–15]), normally as a washcoat with a suitable support on the microchannels. In this respect, zeolites are especially interesting candidates as catalyst supports, on account of their ability to grow as films on a variety of surfaces. In addition, the ion exchange capacity and the microporous structure of zeolites facilitate a homogeneous distribution of metal active sites. In spite of these properties, there are relatively few publications related to zeolite catalysts in microreactors.

* Corresponding author. Tel.: +34 976 761153; fax: +34 976762142.
E-mail address: Jesus.Santamaria@unizar.es (J. Santamaría).

0920-5861/$ – see front matter
doi:10.1016/j.cattod.2007.03.015

The group of Yeung has prepared zeolite microreactors consisting of zeolite synthesised over silicon wafers in which microchannels are made by means of photolithography [16,17]. In this way Ti-silicalite was synthesised over silicon wafers for their application on the epoxidation of 1-pentene [18,19]. They also studied membrane microreactors prepared in multichannel porous stainless steel plates where zeolite films play a separative role without catalytic activity, while the zeolite catalyst nanoparticles were coated on the microchanel [20–22].

The synthesis of zeolites on stainless steel microreactors was studied by Rebrov et al. [23]. They prepared ZSM-5 films over a stainless steel microreactor for the selective reduction of NO to NH_3 with a high yield of product. In addition, Mies et al. [24] investigated the synthesis of zeolite ZSM-5 on molybdenum plates and the scale-up of the synthesis process. They demonstrated a uniform coverage of $14.8 + 0.4$ g/m^2 on a set of 72 molybdenum plates.

Previous works in our laboratory have addressed the advantages of using zeolite films in micro-scale applications [25], including the advantages of coupling reaction and separation at the microscopic level [26]. We have also studied the preparation of zeolite films on a variety of supports, including metallic surfaces [27,28] and ceramic monoliths [29]. In this work, however, we have applied different techniques to optimize the synthesis of zeolite layers on the microchannels of stainless steel microreactors, with the aim of attaining a homogeneous zeolite coating while preserving a high degree of catalyst accessibility.

2. Experimental

2.1. Zeolite synthesis and characterization

Na-ZSM-5 has been prepared, both as powder and also as a film supported on stainless steel microreactors. The microreactors (see Fig. 1) consist of two Plates 50 mm long, 10 mm wide and with a thickness of 2 mm manufactured at Institut für Mikrotechnik Mainz (IMM). In each Plate 14 microchannels (length = 41 mm, diameter = 500 μm) are connected to wider inlet and outlet sections as shown in Fig. 1. Before synthesis the plates were subjected to a cleaning procedure using nitric acid (1 wt%) during 4 h at 60 °C. Afterwards the plates were thoroughly washed with distilled water and cleaned in an ultrasound bath with water and acetone alternatively, followed by drying at 100 °C.

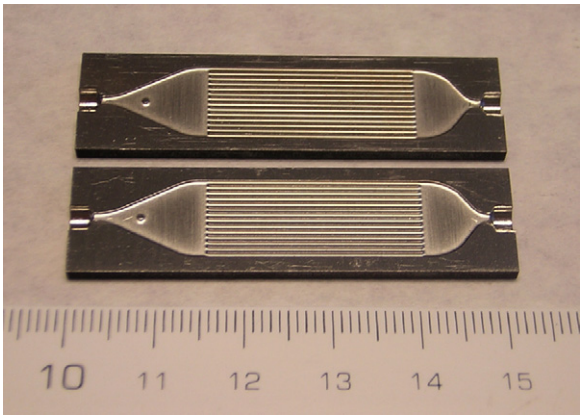

Fig. 1. Images of the starting stainless steel reactor plates showing the microchannels and the inlet/outer sections.

Two different gel compositions were employed for the synthesis of Na-ZSM-5. In gel Z5-1 the molar composition was $21SiO_2{:}X \times 987H_2O{:}3NaOH{:}1TPAOH{:}0.105Al_2O_3$; with $X = 1$; a more diluted gel, Z5-2 (in which $X = 2$) was also employed to reduce homogeneous nucleation and growth of crystals in the bulk of the synthesis solution. The synthesis temperature was varied between 120 and 170 °C and three different synthesis methods were employed, namely, direct liquid phase hydrothermal synthesis, seeded liquid phase hydrothermal synthesis (LHS, also called secondary growth synthesis), and steam-assisted crystallization (SAC). Table 1 summarizes the conditions used during the synthesis of the Na-ZSM-5 films prepared in this work, as well as the zeolite weight gain after synthesis.

2.1.1. Liquid phase hydrothermal synthesis

The stainless steel plate was placed vertically (Fig. 2a) in a teflon-lined autoclave filled with gel Z5-1. The autoclave was placed in a stove and the hydrothermal synthesis was carried

Table 1
Synthesis conditions and weight gain for the zeolite-coated microreactors

Sample	Type of synthesis	Treatment of channel	Gel	Synthesis time	T [°C]	Zeolite gain [mg/g]
MR-1	LHS	None	Z5-1	8 h	170	2.65
MR-2	LHS	Acid	Z5-1	8 h	170	2.08
MR-3	LHS	Seeding	Z5-1	8 h	170	1.07
MR-4	LHS	Seeding	Z5-2	8 h	150	1.71[a]
MR-5	LHS	Seeding	Z5-2	8 h	120	0.43[a]
MR-6	LHS	Seeding	Z5-1	8 h	170	1.14
MR-7	LHS-closed	Seeding	Z5-2	8h + 15 h	150	1.06
MR-8	LHS-closed	Seeding	Z5-2	8h + 15 h	150	0.83
MR-9	SAC	None	Z5-1	4 d	170	0.69[a]
MR-10	SAC	Seeding	Z5-2	8 d	170	0.22[a]
MR-11	SAC	Seeding	Z5-2	16 d	170	0.17[a]

[a] Weight before calcination.

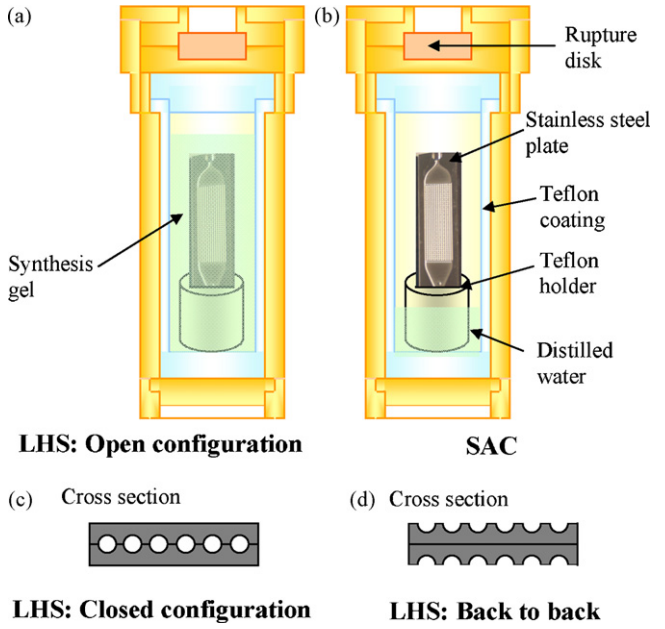

Fig. 2. (a) LHS in an "open" or "back to back" configuration. (b) Steam assisted crystallization method. (c) Cross sectional view of the "closed" configuration used in LHS. (d) Cross sectional view of the "back to back" configuration used in LHS.

out at 170 °C for 8 h. In one case, the microchannels were treated with sulphuric acid to create nucleation sites on the microchannel surface.

2.1.2. Seeded liquid phase hydrothermal synthesis

In this case, silicalite seeds were used together with a more diluted gel to promote secondary growth (growth of the seeds) rather than nucleation and growth of new crystals. The silicalite-1 crystals (ca. 200 nm) used as seeds were obtained previously in a separate hydrothermal synthesis at 125 °C for 8 h using a synthesis gel with the following molar composition: $10SiO_2$:$110H_2O$:1NaOH: 2.4TPAOH. The microchannels were then coated with a 20 g/L suspension of these silicalite seeds using a 1 μL liquid syringe, followed by drying at 100 °C for 3 h. The hydrothermal synthesis of zeolite films was then carried out for 8 h either using gel Z5-2 (at temperatures of 120 or 150 °C) or gel Z5-1 at 170 °C. In the case of the synthesis at 150 °C a second synthesis of 15 h was carried out to increase the zeolite weight in the channel. Both the *closed* and the *back to back* configurations in the vertical position were used in different experiments (see Fig. 2c and d).

2.1.3. Steam assisted crystallization (SAC)

In this procedure the channels were coated with the precursor gel, either Z5-1 or Z5-2, using a liquid syringe, then dried in a furnace at 100 °C. To facilitate crystallization, in some cases, the above described silicalite seeds were used to seed the channel surface before coating with the gel. The plates were placed in a vertical position inside an autoclave in which a known amount of distilled water was poured at the bottom (Fig. 2b). In the subsequent synthesis carried out at 170 °C for 4–16 days water vapour produced the crystallization of the dry gel on the channels.

2.1.4. Post-synthesis treatments

After synthesis of the films by any of the methods described above, the Na-ZSM-5 coated microreactors were calcined in order to remove the template from the zeolite pores. Calcination was performed at 480 °C for 8 h with a heating rate of 0.5 °C/min.

The calcined samples were submitted to a Pt ion exchange procedure. The zeolite powder or zeolite-coated plate was inmmersed in aqueous solutions of $[Pt(NH_3)_4](NO_3)_2$ of variable concentrations at 80 °C for 4 h. Afterwards the plates (or crystals) were calcined at 250 °C for 3 h under a flux of 200 N mL/min of air, followed by reduction at the same temperature in H_2 during 3 h.

Zeolite crystals were characterized by transmission electron microscopy (JEOL-2000 FXII), temperature programmed reduction experiments, and inductively coupled plasma analysis (Perkin-Elmer Elan 6000). The characterization of the zeolite films grown on microreactors included X-ray diffraction analysis (Rygaku/Max System RU 300), scanning electron microscopy and energy dispersive X-ray analysis (JEOL JSM-6400).

3. Synthesis of zeolite films

3.1. Influence of pretreatment of the channel surfaces

The first set of experiments included the samples MR-1 to MR-3, where the films were synthesised using the most concentratred gel Z5-1. In this case, in order to promote growth of the zeolite film on the channel surface (rather than outside the channels), the microchannels were either pretreated with a sulfuric acid solution (MR-2) or seeded with silicalite seeds (MR-3), as described above. Fig. 3 shows the SEM pictures taken after synthesis of MR-1 (no pretreatment), MR-2 and MR-3; the left hand picture in each case shows a back-scattered electron general view of the channels, with the aim of identifying uncoated areas (shown as brighter spots in the back-scattered image). The zeolite grows both inside and outside the channels in the sample that has not been pretreated, and large zeolite agglomerations can be observed, due to homogeneous crystallization in the bulk of the gel, followed by precipitation onto the microreactor plate. Also, the zeolite weight gain in this sample is the highest (Table 1). The back- scattered SEM images also show that for MR-2 and to a lesser extent for MR-1, some bright zones appear inside the channels, indicating that the metal is exposed through gaps in the zeolite film. This is in contrast with the case of the seeded sample MR-3, where the zeolite growth is rather homogeneous and a good coverage of the channels seems to have been obtained. Thus, it can be concluded that seeding promotes an even zeolite film growth and minimizes homogeneous synthesis (zeolite lumps are scarce in MR-3); therefore, it was decided to use seeded synthesis in the subsequent hydrothermal synthesis experiments. In spite of this good result, the objective of minimizing zeolite growth outside the channels was not achieved. As Fig. 3 shows, for the three samples substantial zeolite growth is observed in the channel interspacing.

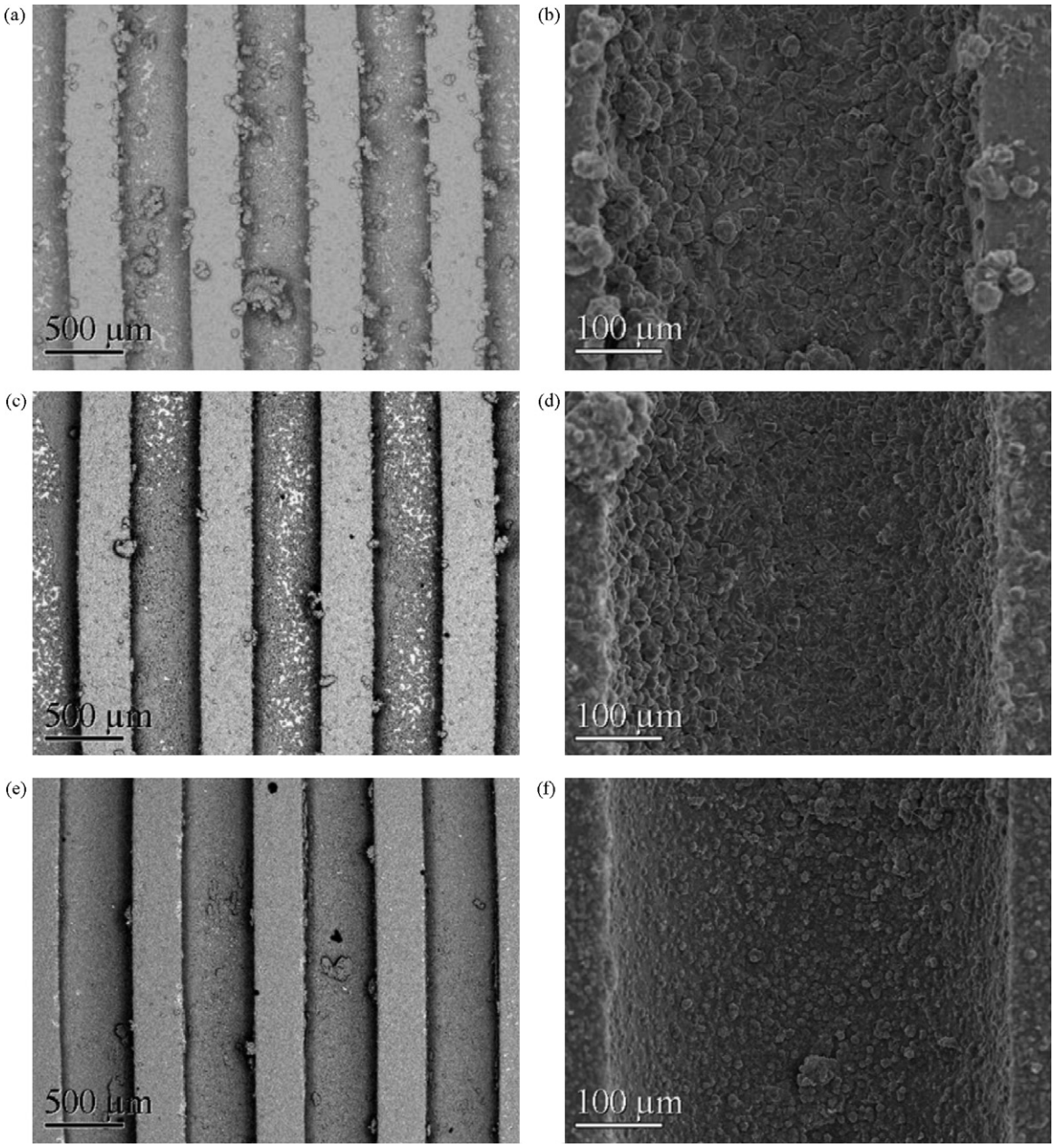

Fig. 3. SEM micrographs: (a), (c) and (e) back-scattered electrons images of samples MR-1, MR-2 and MR-3, respectively; (b), (d) and (f) magnification of a microchannel for samples MR-1, MR-2 and MR-3, respectively.

3.2. Effect of operating conditions (configuration, temperature, gel composition) in the liquid phase hydrothermal synthesis

In order to minimize zeolite growth outside the channels, in some cases (MR-7 and MR-8, Table 1), the plates were placed in the autoclave in the closed configuration (see Fig. 2). As expected, the weight gain corresponding to the zeolite film in this case is lower than in its counterpart when the synthesis was carried out under the same synthesis conditions in an open configuration (MR-4). Thus, the weight gain in MR-7 and MR-8 is roughly half of that in MR-4, in spite of an additional 15 h synthesis period.

It is also interesting to compare samples MR-4 and MR-5, in which the zeolite growth took place on a seeded surface using a diluted gel, but at different synthesis temperatures (150 and 120 °C, respectively). In Fig. 4, the SEM images of sample MR-4 show a ca. 10 μm thick well-intergrown layer coating the channel surface (see Fig. 4a with the general view of the channels in the back-scattered mode, and the inset, with a closer view of a channel), and a thinner film on top of the interchannel spacing (see Fig. 4b showing the cross section of the zeolite coating). On a close-up view of the zeolite film on the channel surface (Fig. 4c), the characteristic morphology of a tightly intergrown c-oriented MFI film is observed; this is in contrast with the view of the zeolite coating grown on the spaces

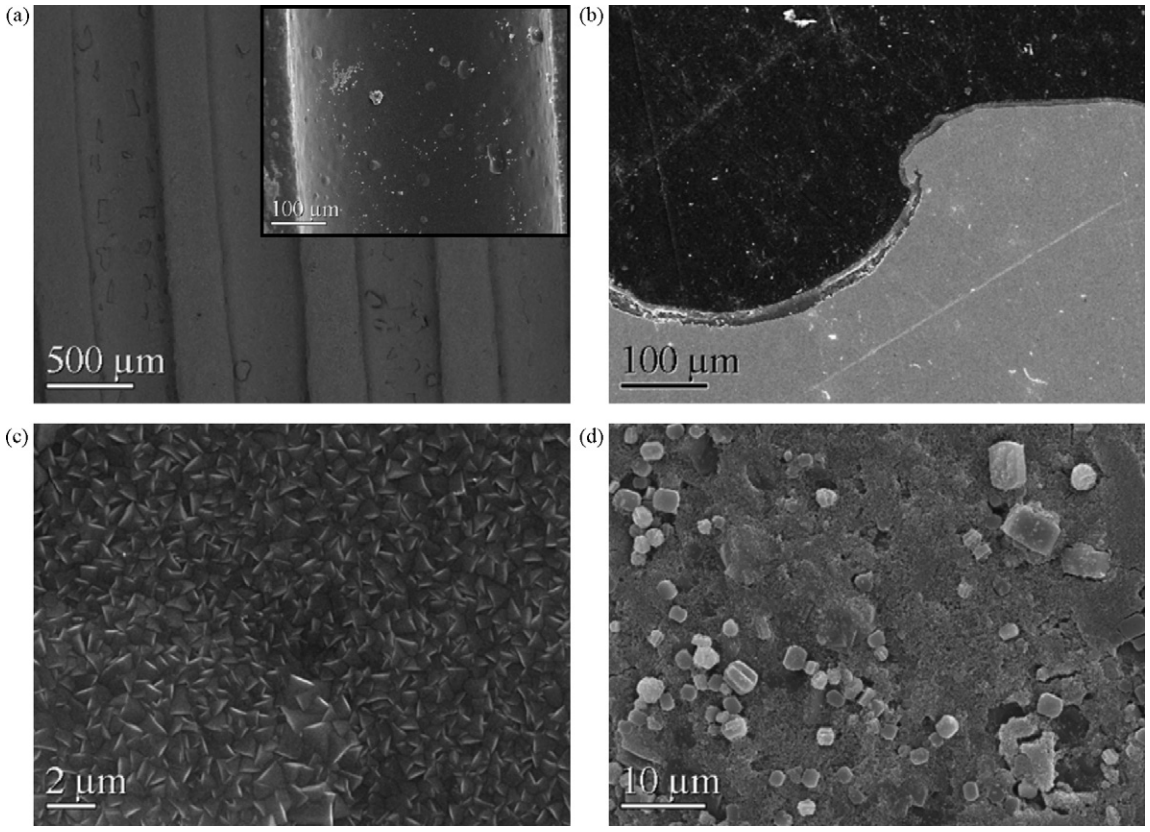

Fig. 4. SEM micrographs of sample MR-4, synthesised at 150 °C. (a) general view of microreactor, the inset is a detail of the channel, (b) cross-sectional view showing the film thickness over the channel and inter-channel region, (c) top view of the zeolite layer inside the microchannels and (d) top view of the zeolite layer outside the microchannel.

between the channels (Fig. 4d), where a less homogeneous crystallization is apparent, with some large b-oriented crystals emerging from the film.

The corresponding images for sample MR-5 are shown in Fig. 5. The backscattered electron micrograph in Fig. 5a, and also the cross-section view (Fig. 5b) indicate that at 120 °C there is little zeolitic material synthesized outside the channels. In spite of this (Fig. 5d), some zeolite crystals are still visible in the interchannel spaces. The crystallization on the channel surfaces is still very good, as shown in Fig. 5c, where a layer of c-oriented MFI crystals typical of secondary growth can be observed; however, the amount of zeolite synthesised is lower, as shown in Table 1, and the crystals are smaller.

Table 2 compares the film thicknesses measured both inside and outside the channels for two plates coated with zeolite films prepared at different synthesis temperatures. As could be expected from the weight gain data in Table 1, the thickness of the film is greater in both regions for sample MR-3 (synthesized at 170 °C), which presents thicknesses above 5 μm. However, the main differences concern the relative thicknesses of the films grown inside and outside the channels for both samples. Thus, for the film prepared at 120 °C using gel Z5-2, the thickness of the zeolite layer inside the channels is larger than outside, while the opposite is true at 170 °C, using gel Z5-1. This indicates that the conditions used for the synthesis of sample MR-5 (lower concentration of the zeolite gel and lower synthesis temperature), favour the preferential growth of zeolite films on the seeded surface of the channels, even though the formation of a zeolite coating in the channel interspace was hindered but not avoided.

Table 2
Layer thickness of samples MR-3 and MR-5

Sample	Gel	T [°C]	Thickness inside the channel [μm]	Thickness outside the channel [μm]
MR-3	Z5-1	170	5.0 ± 0.7	6.3 ± 0.6
MR-5	Z5-2	120	3.4 ± 0.9	1.6 ± 0.1

3.3. Steam assisted crystallization method (SAC)

The steam-assisted crystallization method is often associated with slower synthesis processes and with a lower crystallinity of the zeolite films; however, it seems ideally suited to obtain a selective growth of the zeolite film in the desired zones of the support: since there is no gel deposited outside the channels and contact with a liquid phase is avoided, it is possible to obtain zeolite growth exclusively inside the microreactor channels.

Fig. 6 shows SEM micrographs of the samples MR-9, MR-10 and MR-11, with crystallization times of 4, 8 and 16 days, respectively. In samples MR-10 and 11, the channel surface was seeded before synthesis. In both, seeded and unseeded synthesis the procedure involved filling the channels with the synthesis

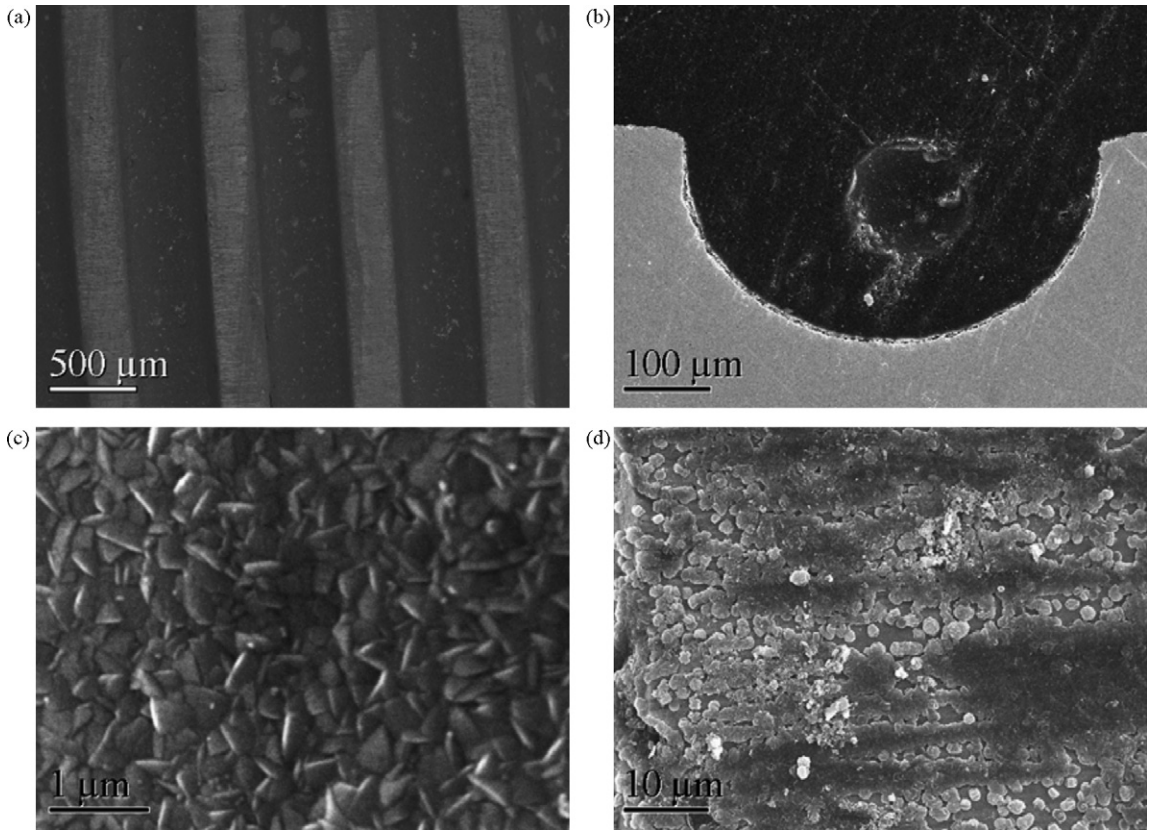

Fig. 5. SEM micrographs of sample MR-5, synthesised at 120 °C. (a) General view of microreactor, (b) cross-sectional view, (c) top view of the zeolite layer inside the microchannels and (d) top view of the zeolite layer outside the microchannel.

gel, then drying at 100 °C before performing the SAC process. Since sample MR-9 was prepared using the concentrated gel (Z5-1), while MR-10 and 11 were prepared with gel Z5-2, the amount of material in MR-9 at the start of the SAC process was larger, producing a thick layer of dry gel inside the channels. The ensuing crystallization time of 4 days was not enough to produce the zeolitization of the gel and only a few crystals were formed on top of the layer while the rest remained largely amorphous (Fig. 6a). In addition large cracks were formed during the heating/drying process of this thick layer (Fig. 6b).

In view of these results, for samples MR-10 and MR-11 the diluted gel Z5-5 was used to fill the channels in order to decrease the amount of material inside the pores, zeolite seeds were added to help crystallization of the gel, and SAC time was increased to 8 or 16 days to allow completion of the crystallization process. Fig. 6c, e and g correspond to the intermediate SAC time of 8 days. The back-scattered electron image of Fig. 6c clearly indicates that the presence of zeolite deposits in the spaces between the channels has been avoided by the use of the SAC method, while a good coverage of the channel surfaces seems to have been obtained. However, a closer look at the zeolite-coated channel surfaces (Fig. 6g) reveals that only partial zeolitization of the gel has occurred: while numerous zeolite crystals can be observed on the gel external surface, considerable amounts of untransformed gel are still present between the crystals.

Increasing the SAC time to 16 days does not increase the amount of zeolite formed, since in the SAC method all the crystallisable material is deposited at the beginning of the process; thus, the weight gain after synthesis is comparable for samples MR-10 and 11 (Table 1). However, the longer crystallization time results in significant changes in the structure and crystallinity of the zeolite film. The back-scattered electron image (Fig. 6d) again shows that, as in the case of MR-10, there are no zeolite deposits outside the channels; however, in this case the appearance of the channel surface is lighter, suggesting some contribution of the underlying metal. The magnifications of this area (Fig. 6f and h) present considerably differences with the corresponding figures after an 8-day SAC synthesis (Fig. 6e and g). The 16-day synthesis produces a well-crystallized zeolite layer homogeneously coating the channel surface, without traces of unconverted gel. In addition, the crystals are well developed and generally maintain their individuality (compare to the intergrown layers obtained with LHS, Figs. 4c and 5c), which would be advantageous from the point of view of catalyst usage in a microreactor. Finally, some micron-sized spaces between the silicalite crystals can be observed, exposing the metal surface underneath, which would explain the brighter appearance of Fig. 6d.

3.4. Pt ion-exchange characterization

As explained in the experimental section, samples of ZSM-5 crystals were exchanged with Pt with the aim of studying the suitability of this method and the distribution of Pt inside the

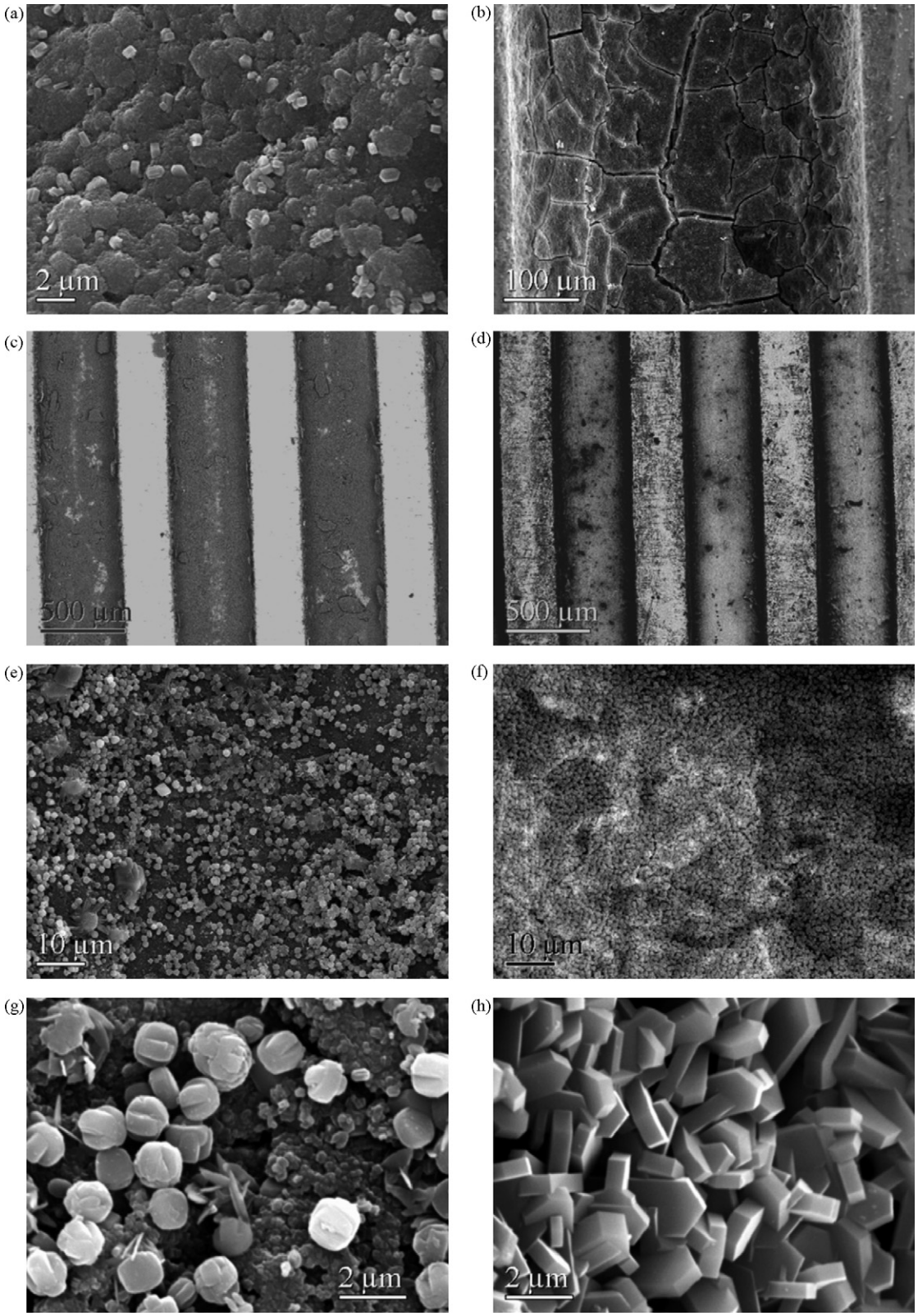

Fig. 6. SEM micrographs of samples prepared by the SAC method: (a) and (b) MR-9, 4 days synthesis; (c), (e) and (g) MR-10, 8 days synthesis; (d), (f) and (h) MR-11, 16 days synthesis. Fig. 6c and d are back-scattered electron images.

zeolite structure. Different Pt loads can be obtained depending on the operating conditions (temperature, impregnation time and concentration of Pt precursors), as shown in Table 3. A temperature-programmed reduction (TPR) experiment with H_2 was performed over a sample of crystals, before the reduction treatment, which yielded the temperatures at which the different Pt species present after catalyst calcination are reduced to metallic Pt. The result of the TPR experiment is

Table 3
Zeolite gain (after the ion-exchange treatment) and Pt content (as wt.% relative to the zeolite) determined by means of EDX (microreactors) and ICP (ZSM-5 crystals)

Sample	Weight of zeolite [mg]	Pt [wt.%]
MR-6	22.7	1.7
MR-7	19.0	4.2
MR-8	17.0	0.64
ZSM-5 crystals	112.6	1.7

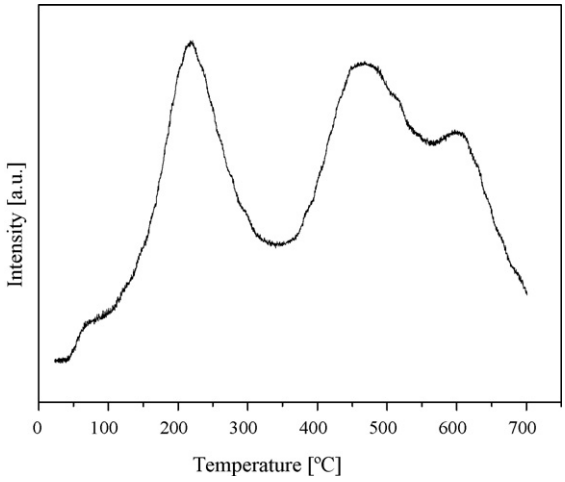

Fig. 7. TPR results for a sample of Pt-exchanged ZSM-5 crystals.

shown in Fig. 7 and it can be seen that there are three different reduction peaks centered at 218, 470 and 600 °C, respectively, that could correspond with the three ion exchange positions α, β and γ of the ZSM-5 framework [30]. The α-type Pt ion exchange postitions are the most accessible to the H_2 because they are located in the main straight channels of the zeolite, thus being reduced at the lowest temperature, while the less accessible β and γ positions become reduced at higher temperatures. The TPR results indicate that a temperature of

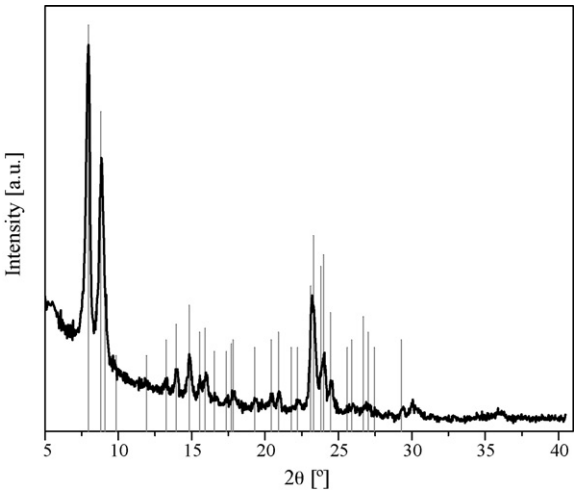

Fig. 9. X-ray diffractogram for sample MR-9 after ion-exchange. Vertical lines correspond to the MFI pattern.

250 °C is enough to reduce most of the α-type Pt ions that are the most accessible and thus the most active sites. Using a higher reduction temperature, up to 700 °C, would activate the remaining exchanged Pt (β- and γ-type) but at the expense of causing the sintering of the metal and the loss of catalytic activity [31].

Pt-exchanged ZSM-5 crystals were also examined by TEM. In Fig. 8a (inset), the typical MFI morphology of several Pt-ZSM-5 crystals can be appreciated. The Pt nanoparticles are distributed throughout the ZSM-5 crystal (main part of Fig. 8a), and as Fig. 8b shows, the size of these Pt particles is around 10 nm. The results of XRD analysis carried out on a zeolite-coated microreactor (MR-9) after the ion-exchange procedure are consistent with this description. Fig. 9 shows that the only reflections present in the XRD pattern are those corresponding to MFI zeolites. The ion-exchange treatment does not seem to affect the crystalline structure of the ZSM-5 films, and the fact that no peaks corresponding to either metallic Pt or Pt oxide

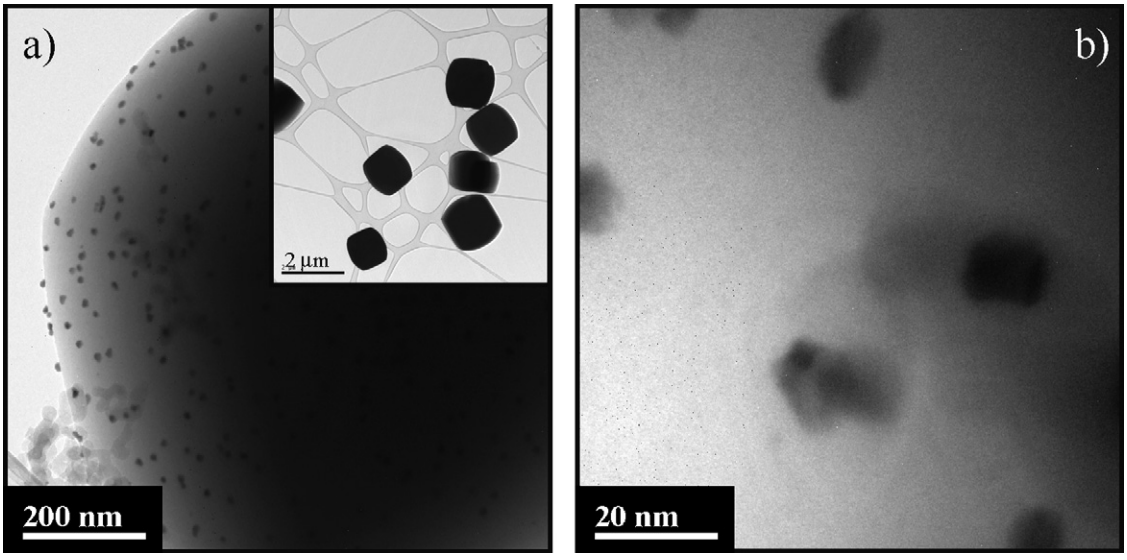

Fig. 8. TEM images of a sample of Pt-exchanged ZSM-5 crystals.

were detected indicates a good dispersion of the Pt aggregates throughout the zeolite film.

4. Conclusions

ZSM-5 films can be grown on the channels of stainless steel microreactors using liquid phase hydrothermal synthesis and steam-assisted crystallization. The former method gives rise to a considerable zeolite load in the form of a film with a thickness of several microns, and a high degree of crystal intergrowth. However, it seems difficult to avoid part of these films forming on the spaces between the microreactor channels. On the other hand, the SAC method requires longer synthesis times, but under suitable conditions leads to well-crystallized thinner zeolite films whose growth is confined to the channel spaces. Once the zeolite films are formed, Pt can be introduced by conventional ion-exchange procedures, producing a homogeneous distribution of Pt in the zeolite films.

Acknowledgements

Financial support from DGA and MEC, both in Spain is gratefully acknowledged.

References

[1] K.F. Jensen, Chem. Eng. Sci. 56 (2001) 293.
[2] K. Schubert, J. Brandner, G. Fichtner, G. Linder, U. Schygulla, A. Wenka, Microscale Therm. Eng. 5 (2001) 17.
[3] A. Gavriilidis, P. Angeli, E. Cao, K.K. Yeong, Y.S.S. Wan, Chem. Eng. Res. Des. 80 (2002) 3.
[4] V. Hessël, H. Löwe, Chem. Ing. Technol. 74 (2002) 185.
[5] K. Jähnisch, V. Hessel, H. Löwe, M. Baerns, Angew. Chem. Int. Edit. 43 (2004) 406.
[6] G. Kolb, V. Hessel, Chem. Eng. J. 98 (2004) 1.
[7] L. Kiwi-Minsker, A. Renken, Catal. Today 110 (2005) 2.
[8] O. Wörz, K.P. Jäckel, T. Richter, A. Wolf, Chem. Eng. Technol. 24 (2001) 138.
[9] G. Veser, Chem. Eng. Sci. 56 (2001) 1265.
[10] O. Wörz, K.P. Jäckel, T. Richter, A. Wolf, Chem. Eng. Technol. 72 (2000) 460.
[11] E.V. Rebrov, M.H.J.M. de Croon, J.C. Schouten, Catal. Today 69 (2001) 183.
[12] K.K. Yeung, A. Gavriilidis, R. Zapf, V. Hessel, Catal. Today 81 (2003) 641.
[13] O. Goerke, P. Pfeifer, K. Schubert, Appl. Catal. A: Gen. 263 (2004) 11.
[14] G. Kolb, R. Zapf, V. Hessel, H. Löwe, Appl. Catal. A: Gen. 277 (2004) 155.
[15] G. Kolb, H. Pennemann, R. Zapf, Catal. Today 110 (2005) 121.
[16] Y.S.S. Wan, J.L.H. Chau, A. Gavriilidis, K.L. Yeung, Microporous Mesoporous Mater. 42 (2001) 157.
[17] J.L.H. Chau, Y.S.S. Wan, A. Gavriilidis, K.L. Yeung, Chem. Eng. J. 88 (2002) 187.
[18] Y.S.S. Wan, A. Gavriilidis, K.L. Yeung, Chem. Eng. Res. Des. 81 (2003) 753.
[19] Y.S.S. Wan, J.L.H. Chau, K.L. Yeung, J. Catal. 223 (2004) 241.
[20] S.M. Lai, C.P. Ng, R. Martín-Aranda, K.L. Yeung, Microporous Mesoporous Mater. 66 (2003) 239.
[21] Y.S.S. Wan, K.L. Yeung, A. Gavriilidis, Appl. Catal. A: Gen. 281 (2005) 285.
[22] K.L. Yeung, X.F. Zhang, W.N. Lau, R. Martin-Aranda, Catal. Today 110 (2005) 26.
[23] E.V. Rebrov, G.B.J. Seijer, H.P.A. Calis, M.H.J.M. de Croon, C.M. van den Bleek, J.C. Schouten, Appl. Catal. A: Gen. 206 (2001) 125.
[24] M.J.M. Mies, J.L.P. van den Bosch, E.V. Rebrov, J.C. Jansen, M.H.J.M. de Croon, J.C. Schouten, Catal. Today 110 (2005) 38.
[25] J. Coronas, J. Santamaría, Chem. Eng. Sci. 59 (2004) 4879.
[26] M.P. Bernal, J. Coronas, M. Menéndez, J. Santamaría, J. Chem. Eng. Sci. 57 (2002) 1557.
[27] F. López, M.P. Bernal, R. Mallada, J. Coronas, J. Santamaria, Ind. Eng. Chem. Res. 44 (20) (2005) 7627.
[28] E. Mateo, R. Lahoz, G. de la Fuente, A. Paniagua, J. Coronas, J. Santamaría, Chem. Mater. 16 (2004) 4847.
[29] M.A. Ulla, E. Miro, R. Mallada, J. Coronas, J. Santamaría, Chem. Comm. 5 (2004) 528.
[30] J. Dědeček, D. Kaucký, B. Wichterlová, Microporous Mesoporous Mater. 35–36 (2000) 483.
[31] P.J.F. Harris, E.D. Boyes, J.A. Cairnst, J. Catal. 82 (1983) 127.